

Characterization and modeling of major constituent equilibrium chemistry of a blended cement mortar

J. Arnold¹, D. S. Kosson^{1,a}, K. G. Brown¹, A.C. Garrabrants¹, J.C.L. Meeussen², H. A. van der Sloot³

¹Vanderbilt University, Department of Civil and Environmental Engineering, Nashville, Tennessee, USA

²Nuclear Research and consultancy Group, Radiation and Environment, Petten, Netherlands

³Hans van der Sloot Consultancy, Langedijk, Netherlands

Abstract. Cementitious materials containing ground granulated iron blast furnace slag and coal combustion fly ash as admixtures are being used extensively for nuclear waste containment applications. Whereas the solid phases of ordinary Portland cement (OPC) have been studied in great detail, the chemistry of cement, fly ash and slag blends has received relatively less study. Given that OPC is generally more reactive than slag and fly ash, the mineralogy of OPC provides a logical starting point for describing the major constituent chemistry of blended cement mortars. To this end, a blended cement mortar containing Portland cement, granulated blast furnace slag, fly ash and quartz sand was modeled using a set of solid phases known to form in hydrated OPC with the geochemical speciation solver LeachXS/ORCHESTRA. Comparison of modeling results to the experimentally determined pH-dependent batch leaching concentrations (USEPA Method 1313) indicates that major constituent concentrations are described reasonably well with the Portland cement mineral set; however, modeled and measured aluminum concentrations differ greatly. Scanning electron microscopic analysis of the mortar reveals the presence of Al-rich phyllosilicate minerals heretofore unreported in similar cementitious blends: kaolinite and potassic phyllosilicates similar in composition to illite and muscovite. Whereas the potassic phyllosilicates are present in the quartz sand aggregate, the formation of kaolinite appears to be authigenic. The inclusion of kaolinite in speciation modeling provides a substantially improved description of the release of Al and therefore, suggests that the behavior of phyllosilicate phases may be important for predicting long-term physico-chemical behavior of such systems.

1 Introduction

The extensive incorporation of ground granulated iron blast furnace slag (BFS) and coal combustion fly ash (FAF) to cementitious materials used in barriers for nuclear waste management has heightened the need for understanding the physico-chemical behaviors of the resulting grout and concrete systems under use conditions in the environment and over extended time frames. Blended cements exhibit a high degree of complexity due to the variability of both the source and the processing of the parent materials, yielding end products comprised of a mixture of glassy and

^a e-mail: David.Kosson@vanderbilt.edu

mineral phases. Ordinary Portland cements (OPC) are also complicated materials but are often well-described by thermodynamic equilibrium models [1]. The work presented here represents a preliminary investigation of the applicability of a set of equilibrium phases developed for Portland cement to a blended cement mortar comprised of OPC, FAF, BFS, and quartz sand (QS).

2 Methods

2.1 Material preparation

Backfill grout mortar (BGM) samples for chemical characterization were prepared by mixing ordinary Portland cement, blast furnace slag, coal fly ash, water, and quartz sand in the proportions listed in Table 1, resulting in a water-to-binder (w/b) ratio of 0.45. The formulation of BGM is within the family of compositions used for reducing grouts in nuclear waste management applications [2]. Total elemental composition of the binder materials for major constituents, as determined by X-ray fluorescence spectroscopy (XRF) are given in Table 2.

Each BGM specimen was cast as a slab measuring 15 cm x 30 cm x 5 cm (width x length x height), removed from its mold after 24 hours, and allowed to cure at $98 \pm 2\%$ relative humidity and 25 ± 1 °C in a nitrogen-purged atmosphere. After 30 months of curing, the outer surfaces of the slabs were removed to mitigate the effects of exposed and molded surfaces, and the remaining interior portion of the slab was crushed and sifted to less than 2 mm particle size for use in leaching experiments.

Table 1. Raw material properties of the backfill grout mortar used in this study. Particle size information was determined from particle size information provided by [3].

Material	Abbrev.	Mass %	Density [kg/L]	Mean Particle Diameter [μm]	Median Particle Diameter [μm]
Blast Furnace Slag	BFS	13.48	2.89	3.87	8.12
Type F Fly Ash	FAF	6.62	2.33	6.02	14.90
Type I Cement	OPC	5.88	3.01	4.16	11.30
Quartz Sand	QS	62.25	2.54	590.6	596.45
Water	-	11.76	1.00	-	-

Table 2. Major element composition of the binder materials as determined by XRF, in mass percent. Carbon (C) is reported as total carbon.

Binder	C	O	Na	Mg	Al	Si	S	K	Ca	Fe
BFS	---	38.17	0.13	6.88	3.46	17.06	0.82	0.35	23.75	0.21
FAF	1.50	45.49	0.25	0.62	15.08	24.42	0.04	2.14	0.86	4.98
OPC	2.50	31.34	0.13	0.58	2.15	7.67	1.55	0.38	41.30	2.70

2.2 pH-dependent leaching test

The USEPA Method 1313 [4] pH-dependent liquid-solid partitioning protocol was used to evaluate major constituent concentrations. Forty grams of BGM were added to 400 mL of solution comprised of deionized water plus HNO_3 or KOH/NaOH for acidification or basification, respectively. The quantities of acid and base additions were prescribed such that nine distinct solution pH values,

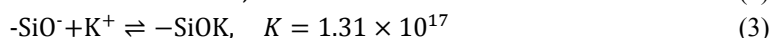
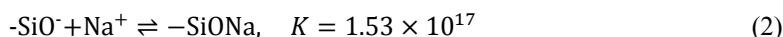
within a tolerance of 0.5 pH units were achieved at the end of the extraction period: 2.0, 4.0, 5.5, 7.0, 8.0, 9.0, 10.5, 12.0, and 13.0. Two replicates of each pH position were achieved, and for the base addition, KOH and NaOH were added to distinct replicates in order to measure the solubility of both Na⁺ and K⁺ at high pH, respectively. Solid samples and leaching solutions were prepared in sealed high density polyethylene bottles with minimal headspace and tumbled end-over-end for a period of 48 hours. Once tumbled, the pH and electrical conductivity of the leachates were measured, and the leachate was vacuum filtered. The filtered leachate was then analyzed for total cation concentrations using inductively coupled plasma optical emission spectroscopy; specific methods, detection limits and quality control procedures used during testing are available [5].

2.3 Geochemical modeling

LeachXS/ORCHESTRA is a geochemical speciation mass transport solver that solves equilibrium speciation via Newton-Raphson minimization of the system of equations composed of the laws of mass action and conservation of mass [6]. The solid phases considered for thermodynamic equilibrium calculations are given in Table 3 with solubility products from Lothenbach, et al. [7]. Additionally, the precipitation of amorphous calcium silicate hydrate (C-S-H) was modeled using the ideal solid solution with Tobermorite-like (C_{0.8}SH_{1.3}) and Jennite-like (C_{1.67}SH_{2.1}) end-members proposed by Kulik and Kersten [8] with end-member solubilities determined by Lothenbach and Winnefeld [9]. Adsorption of K⁺ and Na⁺ onto C-S-H was modeled using partition coefficients fitted to experimental data from a study of alkali uptake onto synthetic C-S-H gel [10]. Assuming a C-S-H surface area of 10.04 m²/kg of C-S-H [11] and a silanol site density of 4.8 mol/nm² [12], and specifying the surface acidity as [12]



the adsorption constants for Na⁺ and K⁺ were found to be



where *K* is the equilibrium constant and -SiO⁻ denotes the silanol site. Adsorption onto -SiO⁻ of the C-S-H is the only mechanism of alkali uptake considered although the alkali filling of interlayer spaces in aluminum-substituted C-S-H proved to be a significant sink for K⁺ and Na⁺ in synthetic gels [13] as well as for Al³⁺ [14,15].

Table 3. Solid phases considered in the BGM assemblage. Species sharing superscripts indicate solid solution end-members. Mineral names are given in cement chemists' shorthand: C – CaO, A – Al₂O₃, S – SiO₂, F – Fe₂O₃, s – S₂O₃, c, CO₂, M – MgO. Amorphous phases are denoted (am) and microcrystalline phases (mcr).

Ca(OH) ₂	CaCO ₃	CaSO ₄ ·2H ₂ O	C ₃ AH ₆	M ₄ AH ₁₀ *****
Mg(OH) ₂	MgCO ₃	C ₄ AsH ₁₂ ***	C ₃ FH ₆	M ₄ FH ₁₀ *****
Al(OH) ₃ (am)	C ₄ Ac _{0.5} H ₁₂ *	C ₄ FsH ₁₂ ***	C ₂ ASH ₈	M ₄ AcH ₉
Fe(OH) ₃ (mcr)	C ₄ Fc _{0.5} H ₁₂ *	C ₆ As ₃ H ₃₂ ****	C ₂ FSH ₈	
SiO ₂ (am)	C ₄ AcH ₁₁ **	C ₆ Fs ₃ H ₃₂ ****	C ₃ AS _{0.8} H _{4.4}	
C ₆ Ac ₃ H ₃₂	C ₄ FcH ₁₂ **	K ₂ Ca(SO ₄) ₂	C _{0.8} SH _{1.3} *****	C _{1.67} SH _{2.1} *****

Reacted fractions of OPC, FAF, and BFS were estimated to be 100, 30, and 80% reacted, respectively based on separate electron microscopy evaluations. Complete or nearly complete reaction of OPC is feasible given the 30-month cure age of the specimen and comparisons with estimates of alite (C₃S), belite (C₂S), aluminite (C₃A), and ferrite (C₄AF) reacted fractions after 2 weeks of hydration obtained from an independent scanning electron microscopy energy dispersive X-ray (SEM-EDX) investigation of the same OPC [16]. The limited reaction of fly ash is similar to

that of other fly ashes reported in the literature. Additionally, limited surface reaction of the Fe-rich FAF particles was observed. Such little reaction reflects the very low concentrations of alkali and alkaline species present in FAF, as presented in Table 2. Eighty percent of slag reacted is similar in magnitude to other reported values [17].

Assuming a single value for reacted fraction of a component material implies a uniform dissolution of each component material, a situation unlikely to occur in reality. At least one study suggests that the dissolution of slag is substantially incongruent [18]. Indeed, in experiments conducted by the authors, when exposed to strongly acidic solution, the BFS off-gassed H_2S (g) and formed a silicate gel. Incongruent dissolution of fly ash particles is also likely given their glassy nature; moreover, the distinct morphologies and compositions of FAF particles suggest distinct intrinsic solubilities among the subtypes of FAF particles. Nonetheless, a uniform reacted fraction is expected to reflect first-order effects of the extent of binder reaction.

3 Results and discussion

Modeled concentrations using the OPC solid phases listed in Table 3 are compared to USEPA Method 1313 leachate concentrations (measured in duplicate) in Figure 1. The resultant equilibrium pH without the addition of acid or base was found to be approximately 12.2

In general, the trends observed in the data are well captured by the equilibrium phases listed in Table 3. The modeled solubility of Ca falls (Figure 1a) within an order of magnitude of the measured values over the pH range of interest ($8 < \text{pH} < 13$). Despite good agreement between measured and modeled Si (Figure 1b) concentrations at pH 10 and pH 12, significant discrepancies are apparent at low and high pH. Several factors may be responsible for these differences. First, the solid solution model of C-S-H which has been developed to describe the formation of C-S-H is assumed here to also describe the dissolution of C-S-H; however, this assumption may not hold if the stoichiometries of C-S-H in this study are outside the range of those for which the C-S-H model end-member solubilities were fitted. Second, silicate phases typically exhibit slow reaction kinetics, and therefore, the experimental results may only approximate the final equilibrium state of the system; this scenario should be more likely near neutral pH where reaction kinetics are typically slowest. The specific adsorption of K^+ and Na^+ onto C-S-H also serve as indicators of the performance of the C-S-H model because the number of silanol adsorption sites is fixed by the total mass of C-S-H present in the system. The trends in solubilities of K^+ (Figure 1c) and Na^+ (Figure 1d) are well captured by the geochemical model (the increasing solubility of K^+ at high pH is an artefact of the KOH addition specified by Method 1313), indicating that the mass of C-S-H formed may be well approximated by this model. Differences in measured and modeled alkali concentrations around pH 8 may reflect a limitation of the homogeneous reacted fraction assumption, particularly for fly ash, the most alkali-rich binder material. Nevertheless, these differences are less than an order of magnitude.

The pH-dependent solubility of Mg is described to within an order of magnitude across the pH range of interest (Figure 1e) which suggests that the hydrotalcite-type is the key solubility controlling phase for this Mg in this system. Strong correlation between total S prediction and experiment (Figure 1d) was found, owing primarily to the precipitation of ettringite.

An important deficiency in the modeling results is the characterization of aluminum. As demonstrated in Figure 2a, the solubility of Al is overestimated by 2 to 3 orders of magnitude between pH 8 and 10. To account for this discrepancy, a number of factors were considered. The precipitation of siliceous hydrogarnet ($\text{C}_3\text{AS}_{0.8}\text{H}_{4.4}$), which forms very slowly at ambient temperatures [19], has been suppressed in the modeling results presented in Figure 2, but it was found that the effect of including $\text{C}_3\text{AS}_{0.8}\text{H}_{4.4}$ was to underestimate the solubility of Al by 2 to 3 orders of magnitude at pH 12 and above. Moreover, $\text{C}_3\text{AS}_{0.8}\text{H}_{4.4}$ was only found to precipitate above pH of about 10.5. Crystallographic characterizations of SCM-replaced Portland cements signify the importance of substitution of Al^{+3} into the silicate tetrahedral network of C-S-H [14,20,21]. Given

the lack of thermodynamic data, the formation of Al-substituted C-S-H (C-A-S-H) was assessed provisionally by partitioning 0.17 moles of Al^{+3} into every 1 mole of Tobermorite-like end-member and for every 1 mole of amorphous silica formed; this rate of substitution is on the order of experimentally measured values [21]. As demonstrated in Figure 2b and 2d, considering C-A-S-H in this manner results in a redistribution of solid phases signifying that sufficient Al would still be free to precipitate all the Al-bearing phases present in Figure 2b; thus, the solubility prediction of Al is unaffected (Figure 2a and 2c).

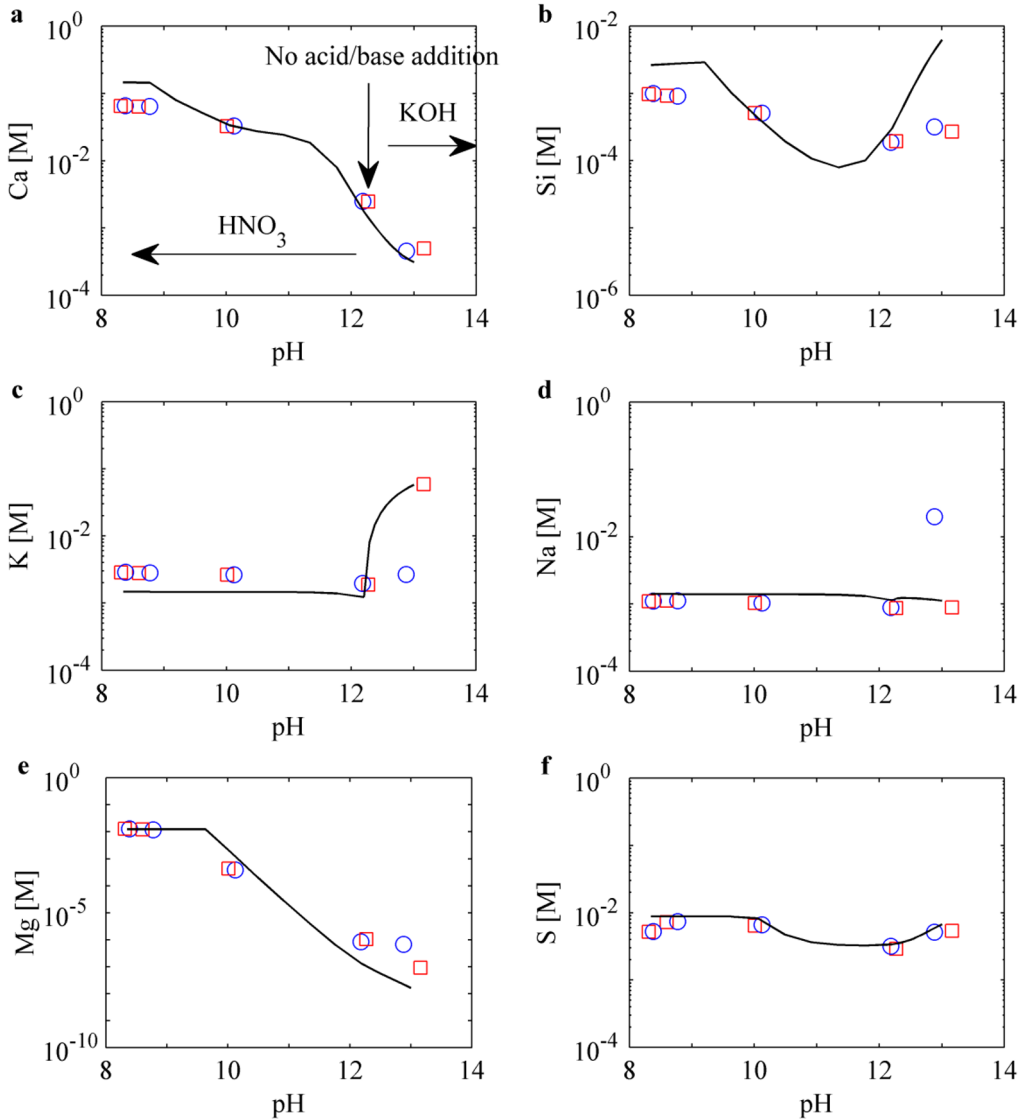


Fig. 1. Comparison of modeled (black lines) and measured (circles and squares) major constituent leachate concentrations (as total dissolved element concentrations) of USEPA Method 1313 performed on BGM. The increasing concentration of K at high pH in c) and of Na in d) are artefacts of the leaching method: independently KOH solution and NaOH were used to adjust the pH of the leachate to a $pH\ 12.5 \pm 0.5$, although only the KOH addition was modeled.

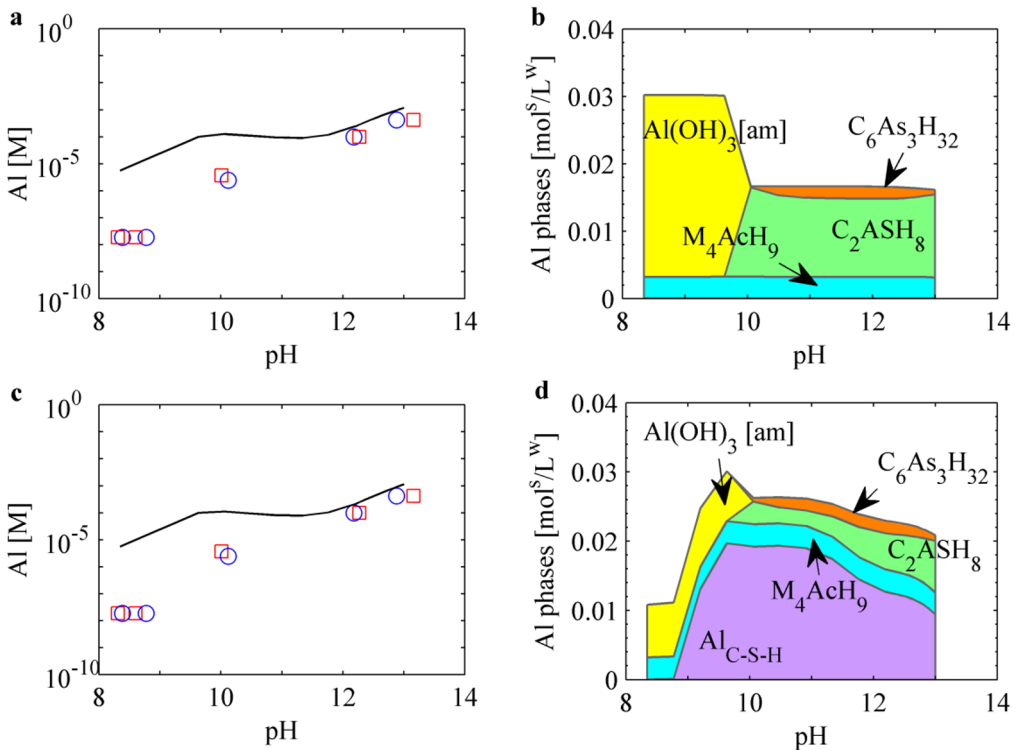


Fig 2. a and c) Comparison of modeled (black lines) and measured (circles and squares) major constituent leachate concentrations and b and d) the concentrations of Al-bearing solid phases. In a and b), no Al uptake by the C-S-H is considered whereas in c and d), 0.17 moles of Al per mole of Si are partitioned into amorphous silica and Tobermorite-like C-S-H end-member.

SEM-EDX analyses provide an indication of additional phases that may play a role in determining Al solubility: a number of phyllosilicates (PS) are apparent within the hydrated BGM after 30 months of curing (Figure 3). To the authors' knowledge, such phases have not been identified previously in blends of cement, slag and fly ash, but their formation is plausible given that PS are clay minerals that commonly form as the result of weathering, diagenesis, and low-grade metamorphism in the natural environment. A number of PS grains are present in the component quartz sand aggregate, but the relative abundance and wide range of sizes of these particles in the BGM material, as well as the spatial (Figure 3a) and stoichiometric correlation of PS to fly ash grains (Figure 3b), suggest that alteration of fly ash is a significant if not primary source of PS formation. Quantitative EDX assay, an example of which is illustrated in Figure 4, indicates that these particles exhibit two basic stoichiometries: that of kaolinite ($\text{Al}_2\text{Si}_2\text{O}_5(\text{OH})_4$) and that of the mica mineral muscovite ($\text{KAl}_2(\text{Si}_3\text{Al})\text{O}_{10}(\text{OH})_2$). Whereas kaolinite is a common weathering product of glassy geologic materials such as volcanic tuff, pure muscovite typically forms in hydrothermal environments and weathers to a class of minerals referred to as illite, a PS of the mica group exhibiting a range of compositions somewhat intermediate between kaolinite and muscovite [22]. In order to examine the effects of PS on the geochemical response of the BGM system, the precipitation/dissolution reactions of kaolinite and a typical illite [23] have been considered, although such an abstraction belies the complexity of most clay mineral systems.

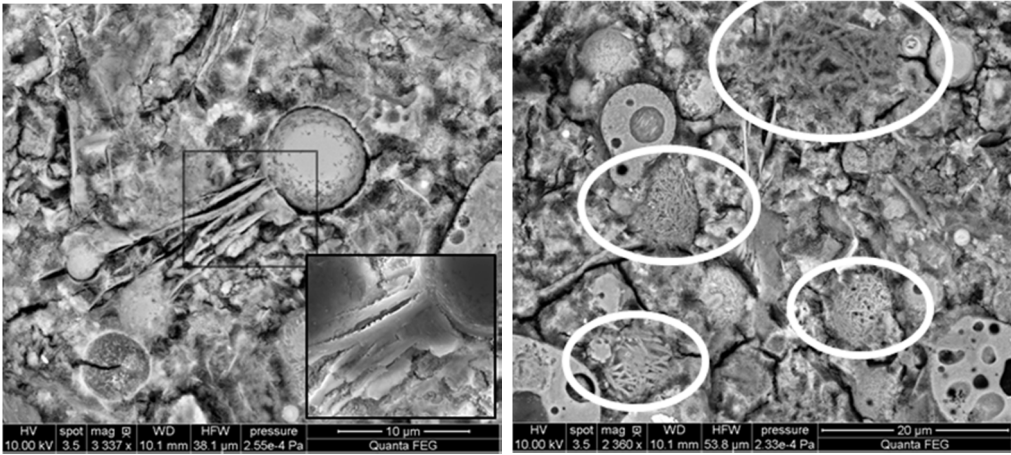


Fig. 3: a) BSE micrograph of kaolinite formation in close proximity to a fly ash particle in the BGM material, with an inset of the secondary electron micrograph of the FAF-PS interface. b) An example of the range of lath-shaped crystals present in the 30-month cured BGM. The spherical nature of the crystal assemblages suggest the in situ reaction of parent FAF particles.

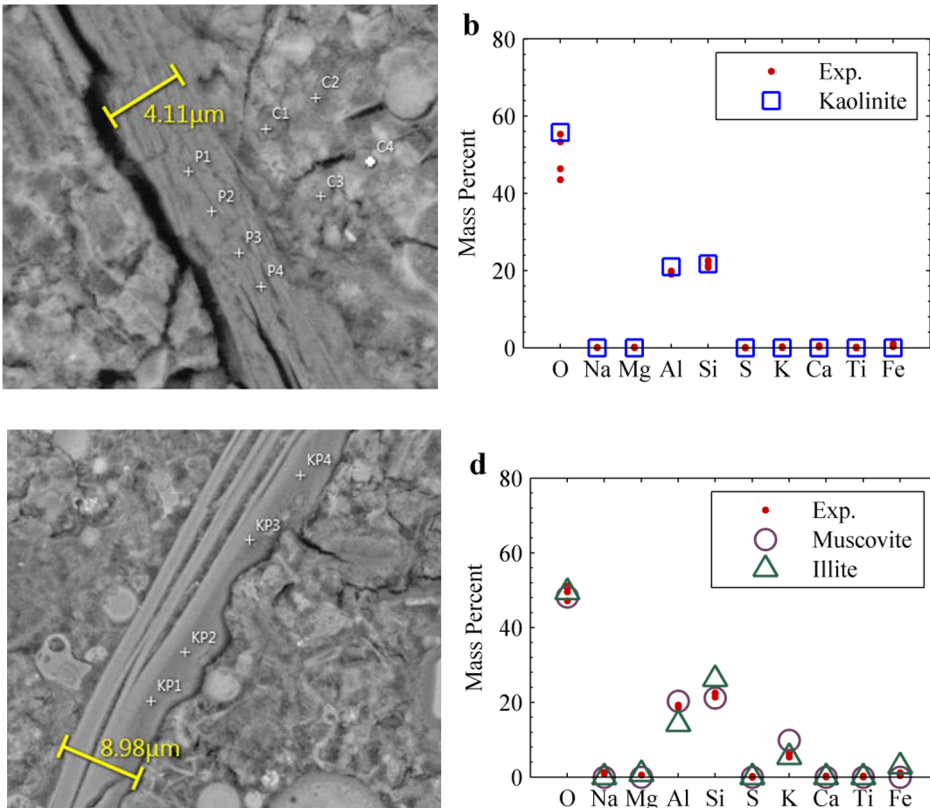


Fig. 4: a) Backscattered electron micrograph of a phyllosilicate presumed to be kaolinite and b) quantitative EDX spectra results for points P1 to P4 (gray error bars) and the theoretical composition of kaolinite (red star). c) Backscattered electron micrograph of a potassic phyllosilicate presumed to be illite and d) quantitative EDX

spectra results for points KP1-KP4 (gray error bars) and the theoretical composition of a typical illite [22] (red star).

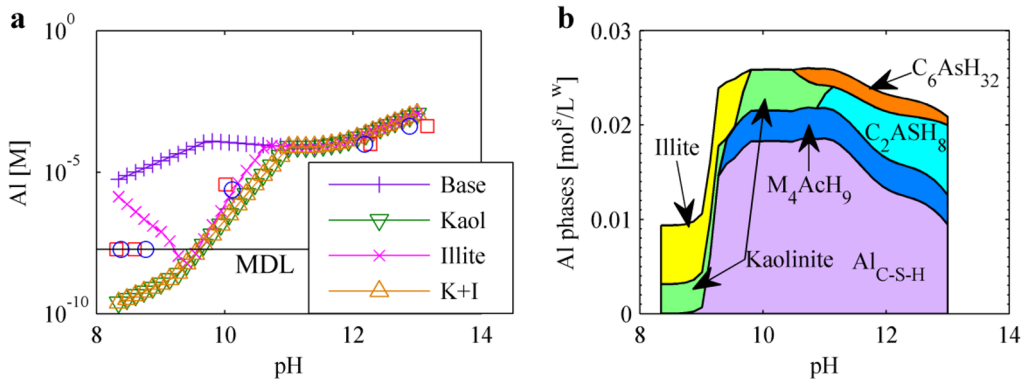


Fig 5. a) Modeled (see legend) and experimental (red squares and blue circles) equilibrium concentration of total dissolved Al with base mineral set (Base) when including kaolinite, illite, and kaolinite+illite (K+I). The experimental values between pH 8 and 9 reflect the method detection limit of the IPC-OES technique. b) The distribution of Al-bearing phases when including kaolinite and illite.

Figure 5a demonstrates the effects of including kaolinite and illite on the equilibrium concentrations of Al. In general, the description of Al solubility below pH 10 is much improved, although underestimated, by considering kaolinite in the thermodynamic equilibrium model, but is virtually unaffected by the inclusion of illite. Including illite in the model prediction drastically reduces the predicted solubility of K below pH 10, however, which perhaps suggests that the illite present in BGM was present in the quartz sand parent material plays a relatively small role in the equilibrium chemistry. That illite may be relatively unreactive in this system is further substantiated by the observation that cracking is apparent near kaolinite grains but not illite grains.

A few words of caution are in order concerning the inclusion of PS in thermodynamic equilibrium models. The first is that PS undergoing dissolution and precipitation often require months to fully equilibrate, depending on the grain size among other factors. Whereas the mortar used in this study has been size-reduced after curing to facilitate testing, a careful study of reaction rate would be necessary to determine if a near-equilibrium condition has truly been reached. Nonetheless, the order of magnitude of solubility within short-term, size-reduced tests should provide a useful indication of the final equilibrium concentration. Second, in the natural environment, the speciation of PS is often complex in that PS sheets are often intermixed across multiple length scales resulting in polymorphs, solid solutions and mixed-layer assemblages such that crystallographic identification and chemical characterization is difficult. Indeed, further evidence for the possibility of impure PS formation is the observation that in Figure 5b kaolinite is unstable above pH of around 11.5 whereas the pore water pH of the unaltered BGM is closer to 12.2; therefore, pure kaolinite should not be present in SEM micrographs of the unaltered BGM. Thus, the fact that the stoichiometry and solubility constant of kaolinite provide a more reasonable Al response is a necessary but not sufficient condition for stating that kaolinite is indeed the solubility-controlling mineral in this pH range for the BGM material. What can be said is that the physical and chemical evidence strongly suggest that Al-bearing PS phases are important for characterizing the behavior of BGM.

Furthermore, a rigorous characterization of the physico-chemical properties of blended cements may require consideration of phases other than those that control solubility. For example, considering the relatively high loading of slag in the BGM mix (52% of the binder, by mass), a substantial portion of fibrillar magnesium silicate hydrates (M-S-H) may be expected to form upon hydration [24], and indeed, a fibrillar product in the reaction rind of BFS is apparent in backscattered electron micrographs, as shown in Figure 6. Encapsulating the M-S-H zone is what appears to be

dense C-S-H; the presence of this sharp compositional interface suggests that migration of constituents from the unreacted slag grain to the surrounding paste would be controlled by the dense C-S-H layer. If M-S-H is effectively sequestered, the thermodynamic behavior of the M-S-H may be of little consequence to the composition of the partial equilibrium assemblage *in situ*; however, cracking, decalcification, and other degradation phenomena, and especially particle size reduction, may degrade the C-S-H barrier, exposing unreacted slag to solution and thereby altering the system equilibrium. Such a phenomenon underscores the need for a mechanistic description of cementitious systems adaptable to a wide range of conditions.

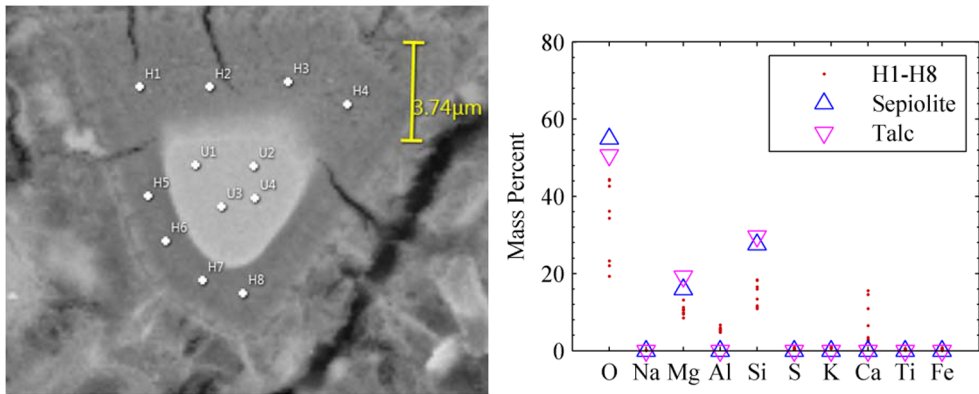


Fig. 6. a) Backscattered electron micrograph of a partially hydrated slag particle in unaltered BGM. b) Comparison of quantitative EDX analyses of the points H1 to H8 with the stoichiometries of sepiolite and talc, two pure phases to which synthetic M-S-H has been likened on the basis of crystallographic similarities [24].

4 Conclusions

A known set of Portland cement solid phases was used to model the equilibrium chemistry of a blended cement mortar. Modeling results generally exhibited the trends and magnitudes observed in a standard equilibrium pH-dependent leaching experiment, aluminum being the notable exception. The exclusion of siliceous hydrogarnet from equilibrium calculations improved the description of Al solubility above pH 10. Below pH 10, the description of Al solubility is greatly improved by the inclusion of kaolinite whose presence has been inferred through SEM-EDX analysis. The presence of potassic phyllosilicates of similar composition to illite and muscovite was also suggested by SEM-EDX analysis; however, the inclusion of illite in thermodynamic equilibrium model resulted in no demonstrable improvement in Al solubility prediction and a worse prediction of K solubility. Whereas kaolinite was not definitively identified as the Al solubility-controlling species below pH 10, the agreement between equilibrium modeling and experiment and the SEM-EDX evidence strongly implicate Al-bearing phyllosilicates as important species that should be considered when describing slag, fly ash and Portland cement blends.

Acknowledgement

This paper was prepared with the financial support by the U. S. Department of Energy, under Cooperative Agreement Number DE-FC01-06EW07053 entitled 'The Consortium for Risk Evaluation with Stakeholder Participation III' awarded to Vanderbilt University. This research was carried out as part of the Cementitious Barriers Partnership supported by U.S. DOE Office of Environmental Management. The opinions, findings, conclusions, or recommendations expressed

herein are those of the authors and do not necessarily represent the views of the Department of Energy or Vanderbilt University.

References

1. D. Damidot, B. Lothenbach, D. Herfort, and F. P. Glasser, *Cement and Concrete Research* **41** (7), 679 (2011).
2. C. Langton, D. S. Kosson, A. C. Garrabrants, and K. G. Brown, Reference cases for use in the Cementitious Barriers Partnership, SRNL-STI-02009-00005, (2009).
3. E. J. Garboczi (Personal communication).
4. USEPA, Method 1313: Liquid-solid partitioning as a function of extract pH using a parallel batch extraction procedure, in *Test Methods for Evaluating Solid Waste, Physical/Chemical Methods (SW-846)*, (2012).
5. D. S. Kosson, L. Stefanski, R. Delapp, P. F. A. B. Seignette, H. van der Sloot, P. Kariher, and M. Baldwin, Interlaboratory Validation of the Leaching Environmental Assessment Framework (LEAF) Method 1313 and Method 1316, (2012).
6. J. C. L. Meeussen, *Environ. Sci. Technol.* **37** (6), 1175 (2003).
7. B. Lothenbach, T. Matschei, G. Möschner, and F. P. Glasser, *Cement and Concrete Research* **38** (1), 1 (2008).
8. D. A. Kulik and M. Kersten, *Journal of the American Ceramic Society* **84** (12), 3017 (2001).
9. B. Lothenbach and F. Winnefeld, *Cement and Concrete Research* **36** (2), 209 (2006).
10. S.-Y. Hong and F. P. Glasser, *Cement and Concrete Research* **29** (12), 1893 (1999).
11. J. J. Thomas, H. M. Jennings, and A. J. Allen, *Cement and Concrete Research* **28** (6), 897 (1998).
12. C. Labbez, I. Pochard, B. Jönsson, and A. Nonat, *Cement and Concrete Research* **41** (2), 161 (2011).
13. S.-Y. Hong and F. P. Glasser, *Cement and Concrete Research* **32** (7), 1101 (2002).
14. I. G. Richardson and G. W. Groves, *Cement and Concrete Research* **23** (1), 131 (1993).
15. B. Lothenbach, K. Scrivener, and R. D. Hooton, *Cement and Concrete Research* **41** (12), 1244 (2011).
16. J. Bullard, P. Stutzman, K. Snyder, and E. Garboczi, Task 7 Demonstrations of Thames for Microstructure and Transport Properties, CBP-TR-2010-007-C2; TRN: US201008%406, (2010).
17. G. Le Saoût, M. Ben Haha, F. Winnefeld, and B. Lothenbach, *Journal of the American Ceramic Society* **94** (12), 4541 (2011).
18. M. Regourd, J. H. Thomassin, P. Baillif, and J. C. Touray, *Cement and Concrete Research* **13** (4), 549 (1983).
19. B. Lothenbach, *Materials and Structures* **43** (10), 1413 (2010).
20. P. Faucon, T. Charpentier, A. Nonat, and J. C. Petit, *Journal of the American Chemical Society* **120** (46), 12075 (1998).
21. G. K. Sun, J. F. Young, and R. J. Kirkpatrick, *Cement and Concrete Research* **36** (1), 18 (2006); X. Pardal, I. Pochard, and A. Nonat, *Cement and Concrete Research* **39** (8), 637 (2009).
22. A. Meunier and B. Velde, *Illite: Origins, Evolution and Metamorphism*. (Springer, New York, 2004).
23. R. C. Routson and J. A. Kittrick, *Soil Sci. Soc. Am. J.* **35** (5), 714 (1971).
24. D. R. M. Brew and F. P. Glasser, *Cement and Concrete Research* **35** (1), 85 (2005).